Soft Matter

PAPER

View Article Online
View Journal

Cite this: DOI: 10.1039/c7sm01518f

Polyelectrolyte scaling laws for microgel yielding near jamming

Tapomoy Bhattacharjee,[a] Christopher P. Kabb,[b] Christopher S. O'Bryan,[a] Juan M. Urueña,[a] Brent S. Sumerlin,[b] W. Gregory Sawyer[ac] and Thomas E. Angelini *[ad]

Received 30th July 2017,
Accepted 6th February 2018

DOI: 10.1039/c7sm01518f

rsc.li/soft-matter-journal

Micro-scale hydrogel particles, known as microgels, are used in industry to control the rheology of numerous different products, and are also used in experimental research to study the origins of jamming and glassy behavior in soft-sphere model systems. At the macro-scale, the rheological behaviour of densely packed microgels has been thoroughly characterized; at the particle-scale, careful investigations of jamming, yielding, and glassy-dynamics have been performed through experiment, theory, and simulation. However, at low packing fractions near jamming, the connection between microgel yielding phenomena and the physics of their constituent polymer chains has not been made. Here we investigate whether basic polymer physics scaling laws predict macroscopic yielding behaviours in packed microgels. We measure the yield stress and cross-over shear-rate in several different anionic microgel systems prepared at packing fractions just above the jamming transition, and show that our data can be predicted from classic polyelectrolyte physics scaling laws. We find that diffusive relaxations of microgel deformation during particle re-arrangements can predict the shear-rate at which microgels yield, and the elastic stress associated with these particle deformations predict the yield stress.

Introduction

The properties that make small hydrogel particles useful in fundamental research also impart them with great technological value.[2] These "microgels" are used not only to investigate the basic origins of jamming and glassy behaviour in soft sphere systems,[3–6] but are also used industrially to control the rheological properties of a multitude of personal care products and lubricants.[7–12] Many of these commercial applications leverage packed microgels' ability to transition smoothly between solid-like and fluid-like rheological behaviours upon the application or removal of shear stress. Recently, this yielding behaviour has been leveraged to 3D print complex soft structures out of silicones, hydrogels, colloids, and living cells inside sacrificial support materials made from jammed microgels.[13–18] Extensive experimental and theoretical research has elucidated the role of particle elasticity and particle–particle interactions in yielding, covering a diversity of materials including packed emulsions, foams, and microgels.[19–22] In the case of microgels, the relationship between particle elasticity, local particle rearrangements, and macroscopic yielding has been explored thoroughly.[3,23–26] However, the connection between polymer physics at the single chain level within microgels, and the phenomenology of microgel yielding has not been established at low packing fractions near the jamming transition. Such a connection would broaden current particle-scale descriptions of yielding and would be a valuable tool in future experimental and industrial efforts, in analogy to the elegant scaling laws of hydrogel material and transport properties, which often depend on single chain structure and dynamics.[27–32]

In this study, we investigate how the established scaling laws of polymer gels can be used to predict the yield stress and cross-over shear-rate in systems of microgels at packing fractions just above the jamming transition. We focus on anionic microgels, which are widely used commercially, and we therefore leverage the pioneering theories of polyelectrolyte physics.[30–32] Using several commercially available microgels and microgels synthesized in our labs, we measure how elastic modulus, yield stress, and cross-over shear-rate depend on polymer concentration, finding that different gels appear to follow different scaling laws that describe two separate regimes of charge density. In both cases we are able to predict yield stress with no adjustable parameters, and we can predict the "cross-over" shear rate between solid-like and fluid-like behaviours to within a small pre-factor. We find that this cross-over shear-rate is controlled by the time it takes the polymer chains within a particle to

[a] Mechanical & Aerospace Engineering, University of Florida, FL-32611, USA. E-mail: t.e.angelini@ufl.edu
[b] Department of Chemistry, University of Florida, FL-32611, USA
[c] Materials Science and Engineering, University of Florida, FL-32611, USA
[d] J. Crayton Pruitt Family Department of Biomedical Engineering, University of Florida, FL-32611, USA

diffusively relax the particle deformations that occur during rearrangement events.

Results & discussion

To investigate the relationship between yielding of jammed microgels and classical polymer physics scaling laws, we perform rheological experiments on commercially available and widely used microgels, as well as a microgel system synthesized in our labs. The commercially available microgels, known as carbomers, are cross-linked copolymer networks of acrylic acid and neutral alkyl-methacrylate monomers; our custom-made microgels are copolymers of methacrylic acid (MAA) and acrylamide (see Methods and materials). The three commercial carbomers used in this study are: Carbopol ETD2020, Carbopol Ultrez10, and Carbopol 980. For brevity throughout the rest of the manuscript, we refer to these as ETD, Ultrez, 980, and MAA microgels. Since all these microgels are made from polyelectrolyte chains, the scaling laws that predict their properties may differ from those of neutral polymer systems depending on charge density and added salt concentration. For both neutral and charged polymers, the scaling laws that predict hydrogel material properties are well established.[28–32] Here, we leverage this understanding of polyelectrolytes to investigate the behaviour of jammed anionic microgels as they yield.

Scaling laws for neutral and polyelectrolyte microgels

The established scaling laws that describe neutral and charged hydrogels were developed for homogeneous, monolithic systems and it is not obvious whether they may be applied to discrete microgels that are jammed together. However, it was previously shown that far above the jamming transition concentration, and within the linear response deformation regime, the elastic modulus of jammed microgels and continuous hydrogels obey the same scaling laws as a function of polymer concentration.[26] In this regime, potential surface interactions like friction or particle interpenetration effects may prevent particle rearrangements such that the mechanics are governed by the properties of the hydrogel material itself. Very much like continuously crosslinked polymer gels, the shear moduli of these jammed microgel systems are set by fundamental polymer behaviour at the single-chain level. In the studies presented here, we explore this phenomenon into lower concentration regimes approaching the jamming limit, which was not previously investigated. Further, we test whether microgel yielding may be predicted using scaling laws that describe neutral and charged bulk hydrogels.

The scaling relationships between shear modulus, G', and polymer concentration, C, for hydrogels made from charged polymers can differ from the neutral polymer case. For fully swollen neutral hydrogels, the material and transport properties are dominantly controlled by a single correlation length known as the mesh size, ξ.[27] Thermally fluctuating polymer chains explore their conformational space within volumes of order ξ^3. These thermal fluctuations resist shear deformations and control the hydrogel elastic shear modulus, given by $G' \approx k_BT/\xi^3$,

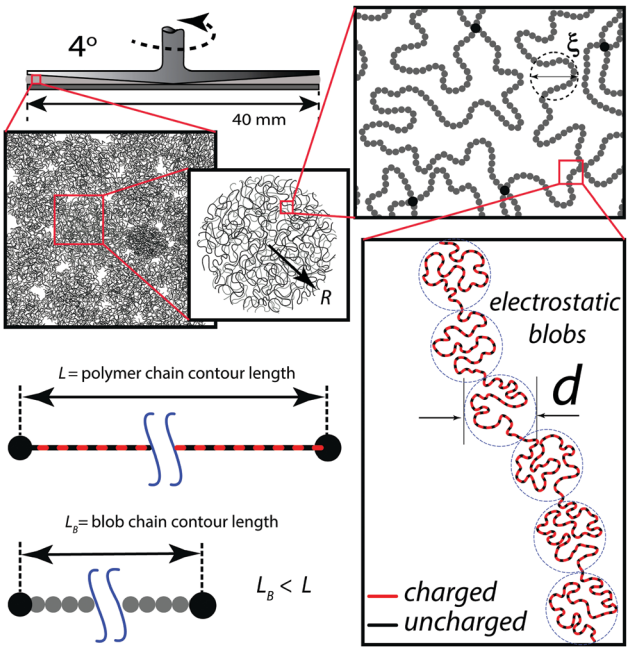

Fig. 1 Illustration of polyelectrolyte microgel hierarchical structure. Polyelectrolyte microgels swell and jam together to form a material that transitions between solid-like to fluid-like behaviors under applied shear stress. In contrast to neutral polymers, the polyelectrolyte backbone exhibits a hierarchical structure that comprises small electrostatic blobs of diameter d which arrange into larger fluctuating chains. The correlation length associated with these chains of blobs is the mesh size, ξ. This re-structuring of the polyelectrolyte backbone effectively reduces the polymer contour length L to a shorter blob chain contour length, L_B.

where k_B is Boltzmann's constant and T is temperature.[28] The scaling relationship between ξ and C for these neutral hydrogels is $\xi \sim C^{-3/4}$. Hence, the elastic shear modulus scales with polymer concentration as $G' \sim C^{9/4}$. The same scaling occurs for fully swollen polyelectrolyte gels in the presence of high concentration added salt, where electrostatic interactions are completely screened.

In contrast to neutral polymer gels, polyelectrolyte gels behave differently under low salt conditions, where charged moieties and counterions influence the polymer backbone configurations and fluctuations.[31] In this regime, the polyelectrolyte backbone behaves like a neutral polymer at the smallest length-scales, up to a cut-off called the electrostatic blob size, d.[33] At length-scales above d, electrostatic blobs repel one another through screened Coulomb interactions and spontaneously arrange into a chain-like configuration (Fig. 1). The Debye screening length sets the persistence length of this larger-scale effective polymer made from electrostatic blobs.[34–37] This fractal re-scaling of polyelectrolytes under low salt conditions modifies fully swollen elastic modulus scaling law, given by $G' \approx (k_BT)/(\lambda\xi^2)$, where λ^{-1} is the re-scaled linear charge density, which corresponds to the projection of all charges along the electrostatic blob backbone. In low-salt polyelectrolyte gels, the concentration dependence of ξ and G' also differ from the neutral gel case, and are given by $\xi \sim C^{-1/2}$ and $G' \sim C^{1}$.[30,32]

Charge density regimes in jammed microgels

To determine which scaling laws describe the material properties of the microgels used here, we measure the relationship between elastic modulus, G', and polymer concentration, C, comparing the data to the scaling predictions described above. For each sample, G' is determined from a frequency sweep test where we apply a low amplitude shear strain (1%) over a large range of oscillatory frequencies. To avoid wall-slip, all rheological measurements employ roughened tools. Over a wide range of polymer concentration, the microgel systems exhibit solid-like behaviours such as a weakly frequency-dependent G' that is larger than G'' over the entire tested frequency range (Fig. 2a). Since the elastic moduli are nearly frequency-independent at low shear amplitudes, we choose G' at 0.1 Hz to be a representative elastic shear modulus. We measure this elastic modulus, G', at many microgel concentrations, C, and construct plots of G' *versus* C. We report G' data down to the lowest concentrations we were able to achieve while remaining in the jammed regime. The MAA, Ultrez, and 980 microgels exhibit strong scaling with C at low concentrations, entering a weaker scaling regime at higher C, as previously observed.[26] By contrast, the ETD microgel exhibits a much weaker scaling at low concentrations. The addition of 3 mM NaCl to the ETD microgel increases the dependence of G' with C, recovering the stronger scaling behaviour seen in the other microgel systems (Fig. 2b and c).

Re-Scaling these G' *vs.* C datasets by their values at the jamming concentration, we find that the data from MAA, Ultrez, 980, and ETD with added salt, all collapse onto a single curve which overlays well with a $C^{9/4}$ power law. By contrast, the data from ETD remains separate and scales more weakly with C at low concentrations, laying closer to the C^1 power law (Fig. 2d). These apparent scaling behaviours correspond to those of the polyelectrolyte low-salt and high-salt regimes, described above. In all experiments, the mass ratio between added NaOH and polymer is constant for all samples across the different types of carbomer, all having a pH of 6.0 ± 0.5 (see Experimental section). Similarly, the MAA system swells most strongly at pH 6.0. At this pH, the Henderson–Hasselbach equation predicts that 98% of acrylic acid groups are de-protonated in all samples. Thus, we interpret the G' *vs.* C scaling results as a reflection of the different polymers' charge densities, and we therefore refer to the microgels exhibiting high-salt behaviour as "low charge density" and the microgels exhibiting low-salt behaviour as "high charge density." The effect of adding salt to the ETD microgel supports this picture. We were surprised to find that the apparent scaling of G' *vs.* C is consistent with that of fully swollen gels. This regime of behaviour occurs over a small concentration range above the jamming concentration, suggesting that the underlying polymer physics can be described by theories of fully swollen systems, within a narrow window.

To test whether these two groups of jammed microgels yield differently, we employ a traditional yielding characterization protocol: the unidirectional shear test. In these tests, we shear microgel samples in a roughened cone-plate geometry, stepping from high shear-rate to low shear-rate while measuring the shear stress and covering the range of 500 s^{-1} to 10^{-3} s^{-1} (Fig. 3a). To determine the yield stress and other parameters related to yielding, we fit the Herschel–Bulkley model to these data, given by $\sigma = \sigma_y(1 + (\dot{\gamma}/\dot{\gamma}_c)^p)$, where σ_y is the yield stress and $\dot{\gamma}_c$ is the crossover shear-rate.[38] Described in this way, the system transitions between the two limiting behaviours when the viscous stress equals the yield stress.[39] Using this approach, we measure the yield stress and crossover shear-rate at many microgel concentrations, finding that the yielding data of the different microgels collapse into the same two groups that are found in plots of their elastic moduli,

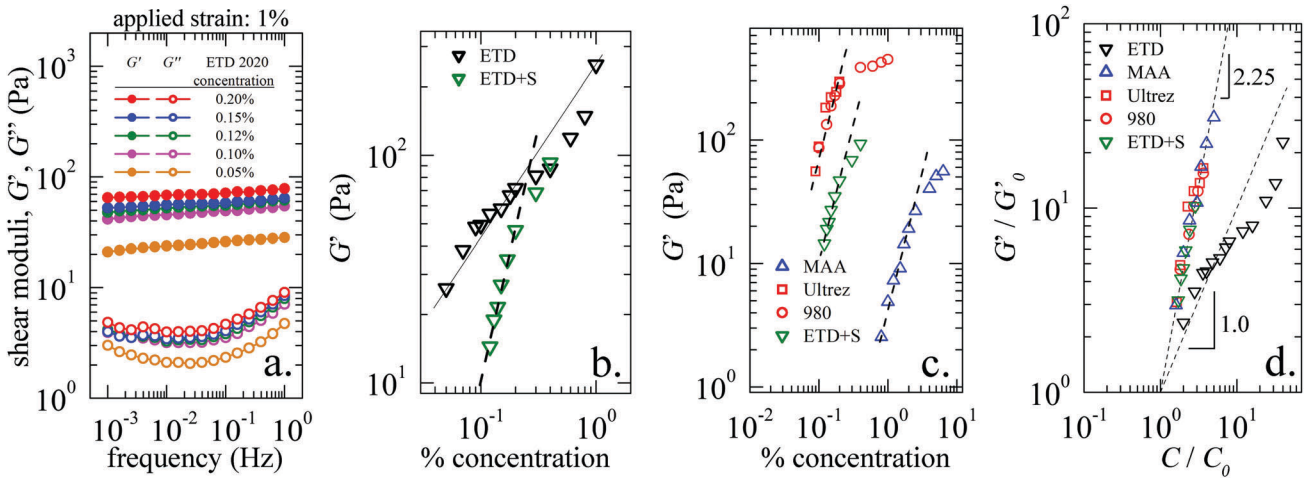

Fig. 2 Rheology and elastic modulus scaling with polymer concentration. (a) We measure the elastic and viscous shear moduli of jammed microgels prepared at many different polymer concentrations. At 1% strain amplitude, over a wide range of oscillatory frequencies, the elastic moduli are nearly independent of frequency and much larger than the viscous moduli. (b) The ETD microgel system exhibits a weaker scaling of G' with polymer concentration, C (black symbols). However, with the addition of NaCl (3 mM), G' exhibits much stronger scaling with C at low polymer concentrations (lines drawn as guides). (c) G' of MAA, Ultrez, and 980 microgels also exhibit strong scaling with C at low polymer concentrations (dashed lines drawn as guides). (d) The datasets collapse into two groups when normalized by G_0' and C_0, the modulus and concentration at the jamming threshold (higher concentration data points omitted for clarity). The data from MAA, Ultrez, 980, ETD with added salt (ETD + S) collapse onto a single curve which scales approximately like $C^{9/4}$; the ETD data without added salt exhibits much weaker scaling, closer to C^1 at low polymer concentrations.

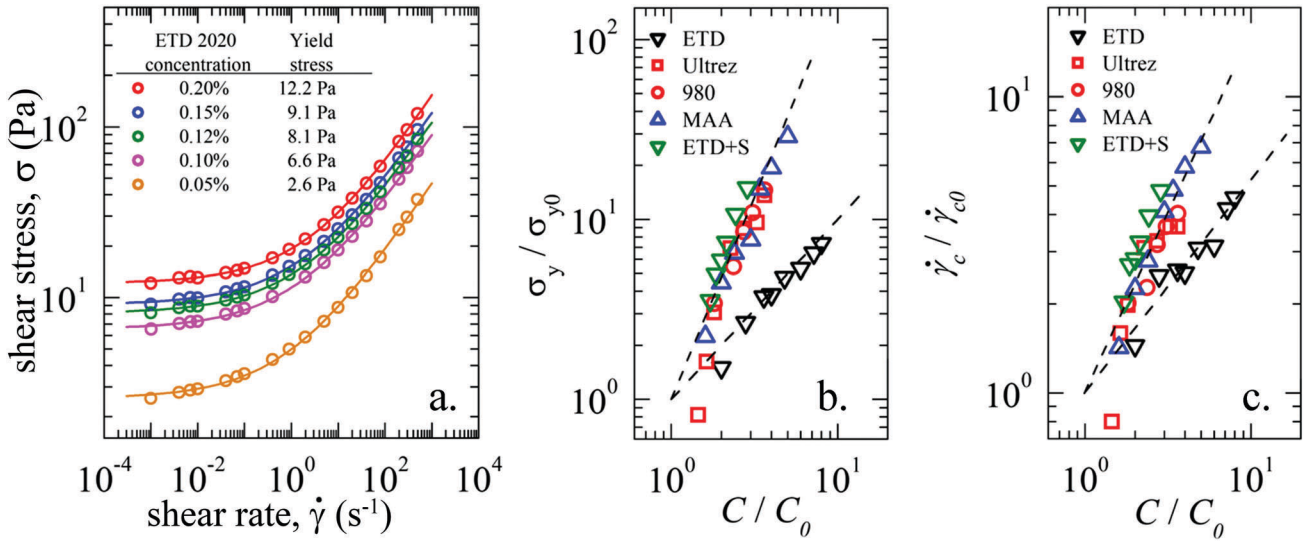

Fig. 3 Yield stress and cross-over shear rate of the jammed microgels. (a) The stress required to maintain a given shear-rate under unidirectional shearing is measured. At high shear-rates, the packed microgels fluidize, exhibiting a shear-rate dependent stress. At low shear-rates, the shear stress is independent of shear-rate. This plateau in stress is the yield stress; the shear-rate at which the viscous stress equals the yield stress defines the cross-over shear-rate. (b) The normalized yield stress of the low-charge density microgels follow a single scaling law with the normalized polymer concentration; the high charge density microgel follows a different scaling law (dashed lines drawn as guides; σ_{y0} and C_0 are the yield stress and polymer concentration at the jamming concentration). (c) The scaling of normalized crossover shear-rate with normalized concentration appear to group by charge density regimes as well (dashed lines drawn as guides; crossover shear rate normalized by its value at the jamming concentration).

when normalized in a similar manner (Fig. 3b and c). We repeated yield stress measurements using oscillatory strain-sweep protocols, finding good correlation between the two methods (see Appendix). While it is interesting that the dataset standing out from the others in Fig. 2 and 3 corresponds to the largest microgels, the data from the apparent low-charge density group cannot be ranked by microgel size, leading us to further analysis, below.

Yield stress prediction from microgel elastic modulus

To predict the yield stress of jammed microgels, we explore two hypotheses; yielding is either controlled by the friction between microgel–microgel interfaces or by the elastic deformations required for re-arranging microgels. Recently, the friction coefficient, μ, at the interface between polyacrylamide hydrogel surfaces was measured at very low interfacial sliding speeds and found to scale inversely with polymer mesh size.[40] It was found that at 17.5% polymer, the highest concentration tested, $\mu = 0.04$; at 3.8% polymer, the lowest concentration tested, $\mu = 0.005$. To test whether this range of friction coefficients applies to charged gels, we perform the same tribological experiments on large-scale poly-(acrylamide-*co*-methacrylic acid) hydrogels (1.9% w/w polymer) formulated to have the same composition as the MAA microgels, finding $\mu = 0.002 \pm 0.0006$ (see Appendix). To test whether this friction could set the yield stress in jammed microgels, we estimate the friction coefficient between microgels by computing the ratio of microgel yield stress to osmotic pressure, Π. Based on our measurements of G' *vs.* C described above, we employ the relationship $G' \approx \Pi$ for fully swollen neutral and charged hydrogels.[30,32] We therefore estimate the friction coefficient to be $\mu \approx \sigma_y/G'$. Computing this ratio from our experimental data and averaging, we find $\mu = 0.13 \pm 0.02$, much higher than the measured friction coefficient for neutral or charged gels. As a point of reference, this is close to the friction coefficient found for polytetrafluoroethylene (PTFE) against hard polished surfaces.[41] Thus, frictional interactions between microgels may not dominate yielding at low packing densities near the jamming transition.

Here we have assumed that the surface properties of bulk gels are the same as those of the microgels. While poly(*N*-isopropylacrylamide)-methacrylic acid microgels have been shown to have a core–shell structure,[42] there are conflicting reports on Carbopol. Micro-rheological measurements suggest that the polymer density is lower at the Carbopol microgel periphery[43] By contrast, small angle neutron scattering data on packed Carbopol ETD 2050 shows no evidence of a core–shell structure or detectable radial variations in polymer density, and were shown to have a random-network structure down to the nano-scale, with some heterogenous domains scattered throughout the microgels.[44] Similar results were found with Carbopol Ultrez 10 microgels.[6] All these observations point to the surface concentration of polymer being the same or lower than the average concentration in each microgel particle. While long polymer loops or dangling chains at high polymer surface density leads to entanglement,[45,46] extremely low surface density of polymer at hydrogel–hydrogel interfaces has been shown to exhibit extremely low friction, entering a regime known as "superlubricity".[47] These results from the literature and our friction data, taken together, suggest that yielding of jammed microgels may be dominated by physical forces different from friction at the gel–gel interfaces.

To test how the elastic energy cost of particle deformations could control yield stress, we ignore friction and examine microgel strain during particle rearrangements. We consider the change in linear dimension in the direction normal to shear, Δl, required for close-packed particles to slide past one

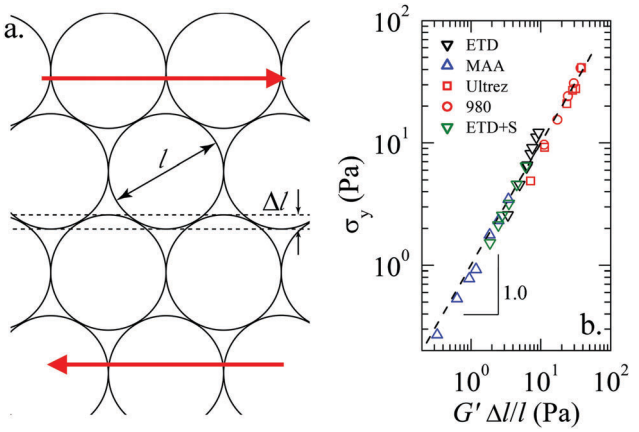

Fig. 4 Prediction of yield stress. (a) The yield stresses of jammed microgels can be predicted by considering the amount of deformation required for close-packed particles to slide past one another in a confined system volume, corresponding to a single particle strain of $\Delta l/l$. (b) The product of this strain (approximately 13%) and measured elastic modulus predicts the measured yield stress for all microgel systems studied here with no adjustable parameters (dashed line corresponds to perfect correlation).

another; one can think of this as $\Delta l/2$ on opposing sides of every particle (Fig. 4a). Using this geometric estimate of intra-particle strain during rearrangement events, we predict $\sigma_y = G'(\Delta l/l)$, where $\Delta l/l \approx 0.13$. Our measurements of the ratio $\sigma_y/G' = 0.13 \pm 0.02$, described above, agree with this prediction (Fig. 4b), as well as the average yield-strain of 0.12 determined from oscillatory tests (Appendix). The data from all microgel systems tested here collapse very well onto the $\sigma_y = G'(\Delta l/l)$ curve with no adjustable parameters. This simple relationship between yield stress and microgel modulus can be re-cast as a function of polymer mesh size using the classical G' scaling laws, described above. As a possible alternative, one could estimate the stress required to change the microgel volume during the same rearrangement process using the bulk modulus instead of shear modulus. However, the bulk moduli of highly charged microgels are three orders of magnitude larger than the shear moduli,[48,49] so the resulting predicted yield stress would be correspondingly large.

Cross-over shear-rate prediction from polymer dynamics

To predict the cross-over shear-rate, $\dot{\gamma}_c$, we search for a characteristic relaxation time (τ) and a characteristic transit time (t) that compete to control the system dynamics, transitioning at $t \approx \tau$. We have compared multiple combinations of transit times and relaxation times (Appendix, Table 1). We empirically find only one combination that predicts our $\dot{\gamma}_c$ data: the whole-microgel transit time competes with the corresponding deformation recovery time to determine the cross-over shear-rate. We discuss this analysis in detail, below.

To predict the amount of time, τ_D, it takes a deformed microgel to relax its shape following a rearrangement event, we employ the single-particle strain described in the last section, $\Delta l/l = 0.13$. Treating these deformation relaxations as limited by the stochastic motion and rearrangement of polymer chains within each microgel, we can write down a diffusion time, $\tau_D \approx \Delta l^2/D$, where D is the single chain diffusion coefficient estimated from the Stokes–Einstein equation. Substituting $\Delta l \approx 0.13l$ and setting $\dot{\gamma}_c^{-1} \approx t \approx \tau_D$, we find

$$\dot{\gamma}_c^{-1} \approx 0.32\frac{\eta l^2 \xi}{k_B T}$$

where k_B is Boltzmann's constant, T is temperature, and η is the viscosity of water.

To write a cross-over shear-rate that depends only on mesh-size, we use the relationship between ξ and polymer concentration to replace l (see Appendix). Similarly, the relationship between ξ and C can be used to write $\dot{\gamma}_c$ in terms of a normalized mesh size, (ξ/ξ_0), where ξ_0 is the mesh-size of microgels at infinite dilution, approximately corresponding to the jamming polymer concentration, C_0, which is experimentally accessible (Appendix). Since C scales differently with ξ for polyelectrolytes in different charge density regimes, we arrive at two different scaling laws for $\dot{\gamma}_c$. For both high and low charge density polymers, this process defines a common parameter $\kappa = (0.32\eta l_0^2\xi_0)/(k_B T)$, where l_0 and ξ_0 are the microgel diameter and mesh size at the jamming concentration. Thus, κ turns out to be the deformation relaxation time-scale for individual microgels at the jamming packing fraction. For high charge-density microgels we find

$$\dot{\gamma}_c \approx \kappa^{-1}(\xi/\xi_0)^{-7/3},$$

and for low charge-density microgels we find

$$\dot{\gamma}_c \approx \kappa^{-1}(\xi/\xi_0)^{-17/9}.$$

We overlay these scaling laws onto the $\dot{\gamma}_c$ datasets according to the groupings by apparent charge density; dimensionless pre-factors between 0.2 and 9 yield good agreement (Fig. 5b). However, since each $\dot{\gamma}_c$ dataset spans less than a decade along both axes, and the $\xi^{-7/3}$ and $\xi^{-17/9}$ power laws are very similar, it is not possible to say with confidence how $\dot{\gamma}_c$ scales with ξ in any individual dataset. Since we expect all four datasets from the low charge density group to follow the same power law, we

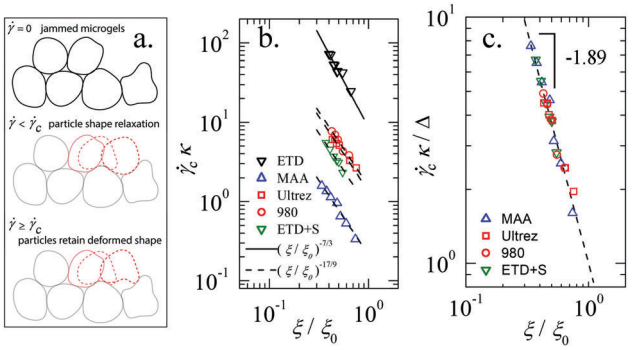

Fig. 5 Prediction of cross-over shear-rate. (a) We predict the cross-over shear rate scaling laws for both low and high charge density polyelectrolyte microgels. If the applied shear-rate is less than the cross-over shear-rate, microgel particles deform to slide past one another slowly enough to diffusively relax their deformed shapes. When the applied shear-rate exceeds the cross-over shear-rate, microgel particles translate so rapidly that they cannot relax their deformed shapes between successive re-arrangements. (b) Our predictions overlay the experimental data with a small pre-factor. (c) All low charge density microgel data collapse onto a single power law, where $\dot{\gamma}_c$ scales with ξ raised to the -1.89 ± 0.02 power or about $-17/9$.

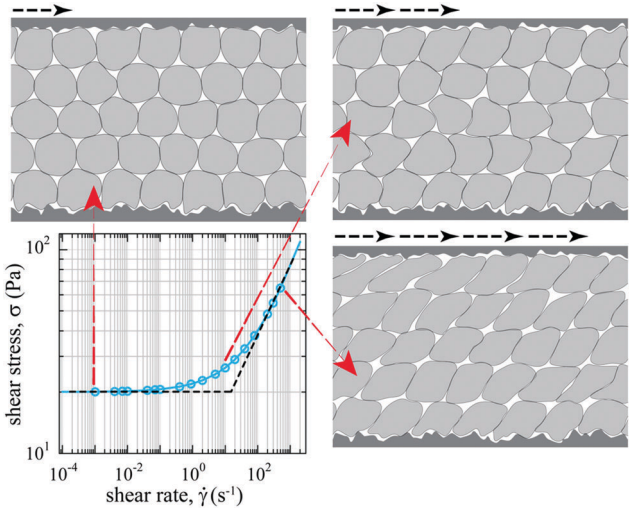

Fig. 6 Rheological regimes in microgel yielding. Microgel yielding is often characterized by measuring shear stress as a function of shear rate. Our results suggest that at low shear-rates, microgels have sufficient time to relax strained shapes limited by diffusive polymer fluctuations, even while re-arranging. At high shear rates, there is insufficient time for strains to relax between re-arrangement events, so shearing continually drives the whole system away from elastic energy minima. The system crosses over between these two extremes when the inter-particle transit time equals the strain relaxation time.

normalize each dataset by a number Δ and collapse the data onto a single curve. Performing an unconstrained power-law fit on the collapsed data, we find that $\dot{\gamma}_c$ scales with ξ raised to the -1.89 ± 0.02 power, very close to the $-17/9$ prediction ($\pm$ is the 95% confidence interval from least-squares fitting). Taken together, these results suggest that when jammed microgels are sheared at rates exceeding the crossover shear-rate, microgel particles translate too rapidly to relax their deformed shapes, never achieving local elastic energy minima, leading the system towards a fluidized state (Fig. 6). To verify whether packed microgels may be viewed as solid-like at very low shear rates even while rearranging, we perform tests in which small amplitude oscillations are superimposed onto unidirectional shear, measuring effective G' and G''. We find that $G' > G''$ at low unidirectional shear rates, crossing over at $\dot{\gamma}_c$, above which $G'' > G'$, reflecting dominantly fluid-like behaviour (see Appendix).

It will be interesting in future work to explore whether this picture of microgel yielding can be used to predict thixotropic behavior, in which a step-wise drop in shear rate is accompanied by an overshoot and recovery in stress over a time-scale called the thixotropic time. Some Carbopols are model non-thixotropic materials[50] while others are slightly thixotropic, exhibiting thixotropic times on the order of seconds.[51] In our studies, all $\dot{\gamma}_c^{-1}$ are between 0.024 s and 10 s, within the range of thixotropic times of the various Carbopols.

Conclusion

In this study, we find that two central properties of jammed microgel systems are set by the polymer mesh-size, similar to how the classical polymer physics scaling laws describe macroscopic gel properties. When a jammed system of microgels is sheared at a rate higher than the cross-over shear-rate, individual microgels do not have sufficient time to relax their shape deformations as they pass by their neighbours. At the cross-over shear-rate, microgels relax deformations as quickly as they re-arrange, just barely packing into their un-sheared configurations. These relaxations appear to be controlled by the polymer chain diffusive motion within microgel particles. In some ways, this behaviour is reminiscent of yielding in jammed emulsions, where particles with negligible friction must deform to re-arrange under shear forces. In contrast to the diffusion controlled relaxation time found here that determines the microgel cross-over shear-rate, the yielding shear-rate in jammed emulsions is determined by how fast the fluid films between drops are drained.[52]

Previous investigations of anionic microgel yielding in colloidal-scale gels at concentrations above jamming show the same G' *vs.* C scaling as found in our measurements of granular-scale microgels.[3] Additionally, the ratio of σ_y to G' in the jamming concentration range was found to be between 0.06 and 0.1, which is comparable to our findings. In other work on Carbopol Ultrez 10, one of the microgel systems studied here, the addition of salt led to a rich set of yielding phenomena at high polymer concentrations; rheological observations suggested that particle cage escape dominates yielding at low salt concentrations and colloidal gel break-up dominates yielding at high salt concentrations.[20] By contrast, our observations of Ultrez 10 microgels at low polymer concentrations and no added salt suggest an extremely simple picture of yielding, which was found to be common among all systems investigated here.

In the work presented here, we prepare microgels at different polymer concentrations and packing densities, studying their behaviour in response to shear forces. At any given polymer concentration, we find that dynamic microgel volume changes are not necessary to explain our experimental data. This interpretation is supported by previous work showing that the microgel bulk modulus is more than three orders of magnitude larger than the shear modulus.[48] Recent investigations of polyelectrolyte microgel compressibility has revealed surprising roles of counterions in highly packed systems. For example, it has been shown that the population of uncondensed counterions in microgels control their swelling and de-swelling.[1,53] Specifically, uncondensed counterions can contribute to the compression of microgels, exerting osmotic pressures larger than the microgel bulk modulus.[54] Thus, we envision work that includes investigating any potential de-swelling with increased packing density in the systems of microgels studied here, and exploring how polymer and ion osmotic pressures may mediate microgel yielding in cases where microgels are shown to change volume under different local shearing conditions.

Materials and methods

Synthesis of low-charge-density polyelectrolyte microgel particles

To synthesize polyelectrolyte microgels, an ethanol solution of 8% (w/w) acrylamide, 2% (w/w) methacrylic acid, 1% (w/w) poly(ethylene glycol) diacrylate (M_n = 700 g mol^{-1}), and 0.1% (w/w)

azobisisobutyronitrile (AIBN) is prepared in a 1 L round bottom flask equipped with magnetic stirring bar. Argon is bubbled through the solution for 30 minutes to remove all air. The deoxygenated reaction mixture is placed into a preheated oil bath set at 60 °C. After about 30 minutes, a white precipitate begins to form. The reaction is heated for an additional 4 hours. At this time, the precipitate is collected by vacuum filtration. The microparticles are then resuspended in 500 mL ethanol and stirred overnight. The microparticles are again collected by vacuum filtration and dried on the filter for ~10 minutes. The particles are dried completely in a vacuum oven at 50 °C overnight to yield a loose white powder.

Microgel preparation

We prepare microgel samples by dispersing dry microgel powder in ultrapure water and mixing using a centrifugal speed mixer at 3500 rpm for 15 minutes. To swell the microgels, we add 10 N NaOH to the microgel suspensions until a pH of 6.0 ± 0.5 is reached. This procedure corresponds to a constant mass ratio between added NaOH and polymer for all Carbopol samples. The swelled microgels are homogenized in a speed mixer at 3500 rpm for 5 minutes. We have systematically studied this mixing protocol, varying mixing time and speed, finding no evidence of damage to the microgels (Appendix Fig. 11). For preparation of successive dilutions, microgels at higher polymer concentrations are diluted with ultrapure water and maintained at the same pH.

Rheological measurements

All rheological measurements except the superimposed unidirectional/oscillatory tests are performed using Malvern Kinexus pro rheometer. Roughened cone and plate tools are used to perform these tests. The conical tool has a diameter of 40 mm with a cone angle of 4°. To load samples between the tools, small volumes of the jammed microgels are poured on the bottom plate at room temperature. The conical tool is then gradually lowered, filling the gap with microgel sample. Excess sample is trimmed from the tool periphery. To measure the elastic and viscous shear modulus, G' and G'', we apply a strain-controlled oscillatory shear of 1% amplitude covering a frequency range of 1 Hz to 10^{-3} Hz. For measuring the yield stresses, we apply a shear-rate controlled unidirectional shear to microgel samples at different rates while measuring the shear stress response. At each shear-rate the sample is sheared for 30 s before recording the stress response.

The superimposed unidirectional shear and oscillation experiments are performed using an Anton-Parr MCR-702 rheometer in stress-controlled mode. Roughened plate–plate geometry is used for these experiments. These tools have a diameter of 25 mm and microgel samples are loaded between the tools to achieve a thickness of 1 mm. To measure the elastic and viscous shear modulus, G' and G'', we apply an oscillatory shear strain of 1% amplitude at a frequency of 1 Hz superimposed with a unidirectional shear covering a shear rate range of 10^{-6} s^{-1} to 1 s^{-1}. At each unidirectional shear rate, the sample is sheared for 60 s before superimposing oscillations.

Data analysis

To obtain the yield stress and cross-over shear rate for each sample, we fit the Herschel–Bulkley model (see Results) to the shear rate *vs.* stress data, using a least-squares fitting algorithm. The associated 95% confidence intervals for yield stresses are approximately ±5% relative to the fitted values; 95% confidence intervals for cross-over shear-rates are approximately ±10% relative to the fitted values. In both cases, these confidence intervals are comparable to the size of the symbols plotted in our figures on logarithmic scales. We therefore omit the confidence intervals from the plots to improve clarity.

Conflicts of interest

There are no conflicts to declare.

Appendix

Measurement of microgel jamming concentration

To find the concentrations at which the different microgels jam, we measure the elastic and viscous shear moduli with oscillatory rheology at 1% strain amplitude and 1 Hz driving frequency. These tests are performed on microgels prepared at a wide range of different concentrations (Fig. 7). We identify the

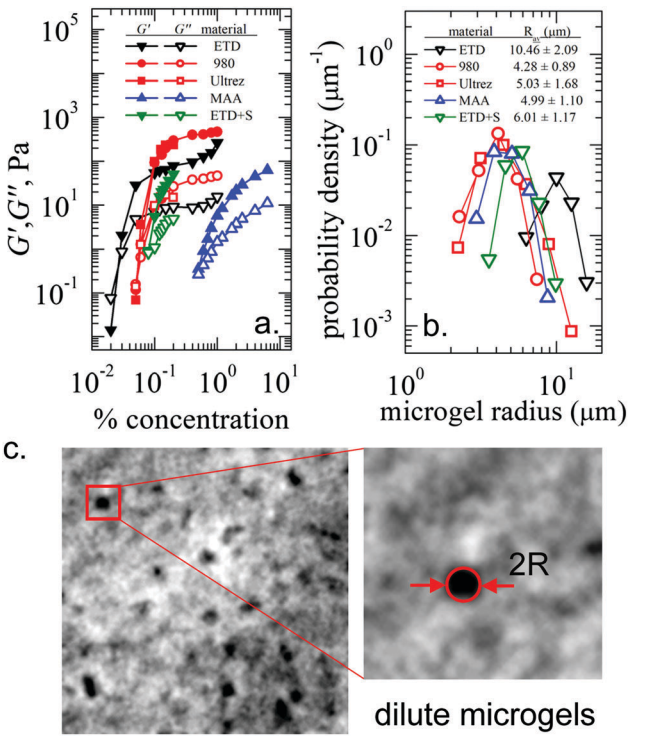

Fig. 7 Jamming concentration and unconfined microgel size. (a) To identify the polymer concentration at which the microgel systems become dominantly solid-like, we measure the elastic and viscous shear moduli at 1 Hz and 1% strain at many polymer concentrations. The concentration at which the elastic modulus equals the viscous modulus determines the jamming concentration. (b and c) To measure the unconfined microgel size, we prepare microgel samples at a dilute concentration and collect images using phase-contrast microscopy. Radii are measured manually and analysed with custom analysis code that computes probability density functions of particle radius. We use the mode of each distribution to determine the unconfined microgel size.

jamming concentration as the point at which the viscous and elastic moduli cross one another; above this concentration the microgel system is solid-like. We find that the low-charge density microgels jam at much higher concentration than the high-charge density microgels.

Measurement of unconfined microgel size

To measure the average diameter of fully swollen microgels, l_0, we prepare samples at concentrations far below the jamming concentration and collect images with a Nikon Eclipse Ti-E microscope using phase-contrast optics. Individual sizes of 80–200 microgel particles are measured manually using Nikon analysis software (Fig. 7b and c). Briefly, particles are identified and outlined manually, approximating them as circular in cross-section to determine radii. These measurements of particle radii are used to generate probability density functions of microgel radii with custom analysis code written in MATLAB. The mode of each distribution is used to determine the typical particle size. We find that the low-charge density microgels are comparable in size to one another; the high-charge density microgels are much larger. Our measurement of the microgel size is consistent with the previously reported results.[44,55]

Polyelectrolyte microgels with added salt

We prepare jammed microgels at 0.2% polymer concentration from Carbopol ETD 2020. With the addition of NaCl at low concentrations, G' of the jammed system is independent of added salt concentration. At high salt concentrations, G' becomes strongly dependent on the amount of added salt ($G' \sim C_{\mathrm{NaCl}}{}^{-3/4}$) (Fig. 8). This behaviour is consistent with that of a fully swollen, high charge density, bulk polyelectrolyte hydrogel, which transitions between the two limiting behaviours with added salt.[32]

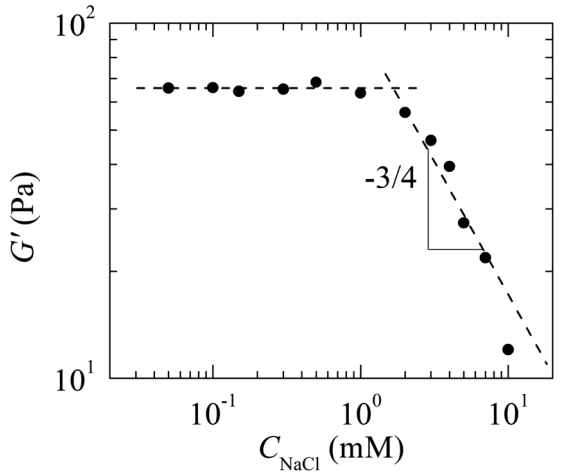

Fig. 8 Salt concentration dependence of ETD 2020 microgels. Jammed microgels at 0.2% polymer concentration are prepared from Carbopol ETD 2020 containing different amounts of added salt. At low salt concentrations, G' is a constant. With increased NaCl, G' decreases, exhibiting a scaling consistent with the $C^{-3/4}$ power law, predicted by polyelectrolyte theory.

Friction measurement at Gemini polyelectrolyte interfaces

To find the coefficient of friction at the interface of two polyelectrolyte gels we prepare a slab and a hemispherical probe of poly-(acrylamide-*co*-methacrylic acid) hydrogels (1.9% w/w polymer) formulated to have the same composition as the MAA microgels. This probe is the rubbed on the slab at a normal load of 1 mN with a reciprocating stroke of 800 μm and a sliding speed of 100 μm s^{-1} on a custom built microtribometer,[40,56–61] following the previously established protocols and analysis methods.[62,63] The free sliding region of the friction loop (dashed box in Fig. 9) was used to calculate the average friction coefficient over 150 reciprocating cycles, which was $\mu = 0.002 \pm 0.0006$. Our experimental uncertainties in measuring friction coefficients are $\mu = 0.0005$.[61]

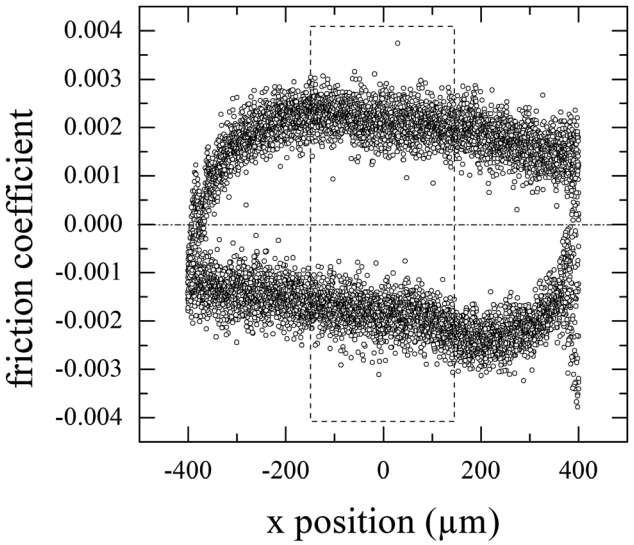

Fig. 9 Friction at the polyelectrolyte hydrogel interface. Two identical surfaces of 1.9 w/w% poly-(acrylamide-*co*-methacrylic acid) hydrogels are slid against each other at a normal load of 1 mN with a reciprocating stroke of 800 μm and a sliding speed of 100 μm s^{-1}. Data from the free sliding region (dashed box) are analysed to find $\mu = 0.002 \pm 0.0006$.

Time-scales in jammed microgel yielding

We have analysed and compared many combinations of different transit times (t) and relaxation times (τ). Examples of t include the time required for a single polymer mesh on one microgel moving at speed v to slide past another polymer mesh on an adjacent microgel, $t \approx \xi/v$. Similarly, the transit time for electrostatic blobs on adjacent microgels is given by $t \approx \mathrm{d}/v$, and the transit time for entire microgels of size l to pass one another is given by $t \approx l/v$. We compare these transit-times to relaxation times. Possibly the simplest relaxation time to consider is the ratio of solvent viscosity to linear elastic modulus, as was previously explored in colloidal and granular-scale gels.[26] We find the predicted relaxation time-scales to be 10^4 times too short. An alternative possibility is the time for a chain of blobs to diffusively explore the mesh size, given by $\tau_\xi \approx (\eta_s \xi^3)/(k_B T)$. Another candidate of τ is the time required for a deformed

microgel to relax its shape through diffusive polymer motion (described in the manuscript body). Alternatively, τ could be the amount of time required for a microgel to swell under its own osmotic pressure. However, since the bulk modulus of charged microgels is more than three orders of magnitude larger than the shear modulus, it is unlikely that microgels will compress and decompress under shear stresses and will always remain at a constant osmotic pressure. Thus, we eliminated this possibility from consideration. In all cases, we approximate the shear-rate to be $\dot{\gamma} \approx v/l$, where v is the difference in speed between neighbouring microgels of size l. This definition of shear-rate assumes that the shear is homogeneous down to the scale of the microgel particles. The cross-over shear-rate, $\dot{\gamma}_c$ is also given by v/l, but under the condition $t \approx \tau$. Solving these combinations of $t \approx \tau$ for $\dot{\gamma}_c$, we find that the combination of the whole-microgel transit time and the deformation relaxation time predicts our data. Interestingly, this cross-over criterion turns out to define a corresponding Peclet number, $\mathrm{Pe} = h^{-1}\tau_D{}^{-1}$, since the competing time-scales are advective and diffusive.

Table 1 Time-scales associated with microgel

Transit time (t)	Relaxation time (τ)
Microgel: $t \approx l/v$	Signal mesh diffusion: $\tau_\xi \approx \frac{\eta\xi^3}{k_B T}$
Single mesh: $t \approx \xi/v$	Deformed microgel diffusive recovery: $\tau_D \approx \frac{6\pi\eta(\Delta l)^2\xi}{k_B T}$
Electrostatic blob: $t \approx d/v$	

Concentration, mesh-size, and microgel diameter scaling

Using established polyelectrolyte scaling laws it is possible to re-cast our analysis in terms of polymer concentration, C, mesh-size, ξ, or particle size, l. For low-charge density polyelectrolyte microgels, mesh size and polymer concentration can be related by

$$\xi \approx \xi_0 \left(\frac{C_0}{C}\right)^{3/4},$$

where C_0 and ξ_0 are the polymer concentration and mesh-size at the jamming packing fraction; we use C_0 as an experimentally convenient reference point. For the data presented in the Results section, $C \geq C_0$, and as the particles compress, their mesh-size decreases. Similarly, the relationship for high-charge density polyelectrolytes is given by

$$\xi \approx \xi_0 \left(\frac{C_0}{C}\right)^{1/2}.$$

These two relationships can further be used to relate particle size to mesh-size by employing $l \sim C^{-1/3}$, which also captures microgel compression with increased C above C_0. Thus, for high charge density polyelectrolyte microgels, we find

$$l = l_0(\xi/\xi_0)^{2/3}.$$

For low charge density polyelectrolyte microgels, we find

$$l = l_0(\xi/\xi_0)^{4/9}.$$

For microgel concentrations beyond the overlap concentration, we infer the mesh-size from low frequency elastic modulus, G' (0.1 Hz). In the case of low-charge density microgels, the mesh-size is calculated from

$$\xi \approx \left(\frac{k_B T}{G'}\right)^{1/3}.$$

In the case of high-charge density microgels, the mesh-size is calculated from

$$\xi \approx \left(\frac{k_B T}{\lambda G'}\right)^{1/2},$$

where, λ is the re-scaled linear charge density, which corresponds to the projection of all charges along the electrostatic blob backbone. Here, we predict the scaling law for $\dot{\gamma}_c$ only to within an unknown multiplicative coefficient; the unknown factor of λ merely re-scales this coefficient. Thus, we set λ = 1 nm and find agreement with our data using a pre-factor of 9. This estimate for lambda is comparable to previous work describing the charge renormalization of acrylic acid.[32,64]

Yielding from oscillatory shear

To measure the yield stress under oscillatory shear with increasing amplitude, we use roughened tools to shear different types of microgels at 0.1 Hz frequency for a wide range of shear strain (1–100%). The stress at the cross over point between the linear regime and non-linear regime of stress–strain response is considered as the yield stress, as previously reported[1] (Fig. 10a). Yield stress measured in this fashion correlates very well with the yield stress measured from unidirectional shear experiments with R^2 = 0.96, though the scatter in the correlation plot reflects differences between these methods on a sample-to-sample basis (Fig. 10b). The average yield strain from these measurements is

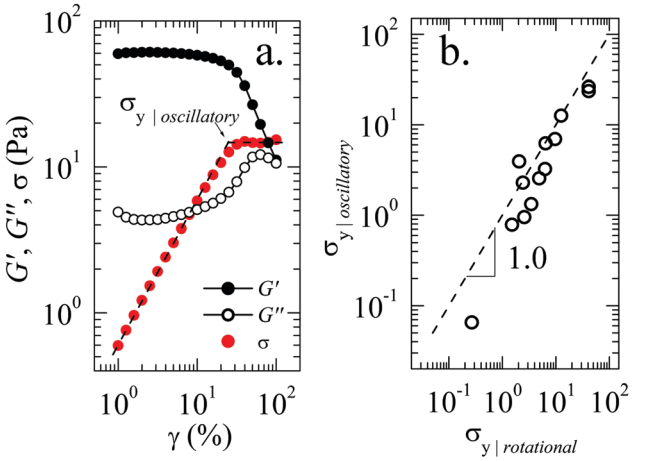

Fig. 10 Yielding under oscillatory shear. (a) Jammed microgel samples are sheared at 0.1 Hz frequency and 1 to 100% strain amplitude. Yield stress is determined by the dramatic change in slope in the stress–strain curve, as previously demonstrated.[1] (b) Yield stress measured from oscillatory rheology correlates with the yield stress measured from unidirectional shear rheology (dotted line represents perfect correlation, which yields R^2 = 0.96 with the data points).

found to be 0.12 ± 0.07, close to the $\Delta l/l$ = 0.13 discussed in the main manuscript. Additionally, these amplitude tests verify that all samples are in the linear viscoelastic at 1% strain and 0.1 Hz, the conditions under which we report G' as a function of polymer concentration.

Microgel mixing and pre-shearing tests

To test whether the yield stress values reported here are affected by the measurement duration, we repeat the unidirectional shear tests described above while varying the time over which instantaneous shear stress data points are averaged. We find little variability with changing this measurement duration; the Carbopol and MAA microgels sheared at 10^{-3} s^{-1} exhibit no apparent changes in shear stress when varying the measurement duration between 30 s to 300 s (Fig. 11a).

To test whether the mixing protocol used in this manuscript affects the measured yield stress, we prepare many samples of Carbopol 980 at 0.2% polymer concentration following different mixing protocols. For all tests, Carbopol 980 powder is speed-mixed in water for 30 min at 600 rpm, then swollen by adjusting the pH to 6.0. After adjusting the pH, additional mixing is performed. For the for first protocol, the sample is speed-mixed for 15 min at 600 rpm (protocol A). The sample from protocol A is then speed-mixed for another 10 min at 600 rpm (protocol B). We find a very small increase in yield stress for the protocol B sample relative to the protocol A sample, suggesting protocol A may not fully homogenize the sample. To test whether mixing at higher speeds damages the microgels and significantly alters the yield stress, the protocol B sample is speed-mixed for 5 min at 3500 rpm (protocol C). A very small increase in yield stress is observed, comparable to the confidence intervals of the data points. To determine whether the effect of high speed mixing differs from that of long-time equilibration, we leave the sample from protocol B at room temperature for 5 days and then speed-mix for another 5 min at 600 rpm (protocol D). We observe no difference between the protocol C and protocol D samples. Finally, to further test if high speed mixing may damage the microgels, the protocol D sample is speed-mixed for another 5 min at 3500 rpm (protocol E). We see a very small drop in yield stress, once again comparable to the confidence intervals of the data points. Compared to the changes in yield stress with concentration and across microgel species, these

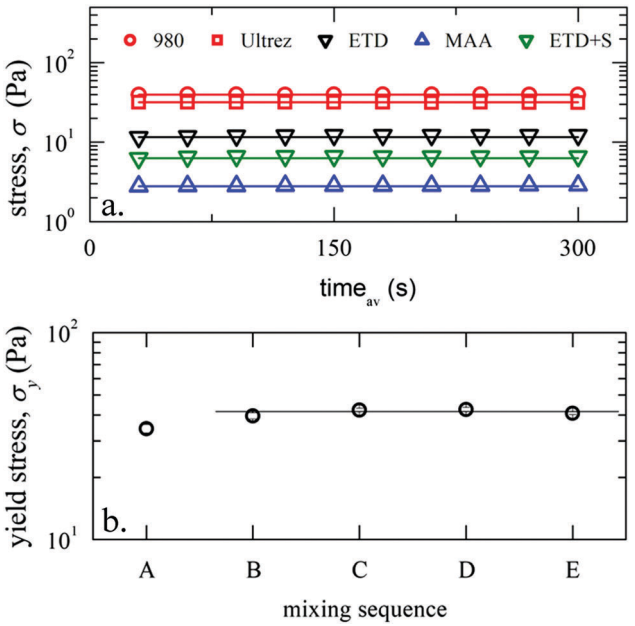

Fig. 11 Shearing and mixing protocols. (a) Microgels prepared from Carbopols and MAA are sheared at 10^{-3} s^{-1}. Stress is measured over different durations, between 30 s to 300 s. The shear stress remains independent of the measuring duration. (b) Carbopol 980 is prepared at 0.2% concentration following five different mixing protocols. Four of these protocols effectively result in same yield stress. For these samples Carbopol 980 powder is speed-mixed in water for 30 min at 600 rpm before adjusting the pH with NaOH. After adjusting the pH, we introduce variation in the mixing process. Protocol A: speed-mixed for 15 min at 600 rpm. Protocol B: sample from protocol A speed-mixed for another 10 min at 600 rpm. Protocol C: sample from protocol B is speed-mixed for another 5 min at 3500 rpm. Protocol D: sample from protocol B is left at room temperature for 5 days and then speed-mixed for another 5 min at 600 rpm. Protocol E: sample from protocol D is speed-mixed for another 5 min at 3500 rpm. Error bars are 95% confidence intervals from fitting the Herschel–Bulkley model to unidirectional shear data as described in the manuscript. Horizontal line illustrates the similarities between data from different protocols.

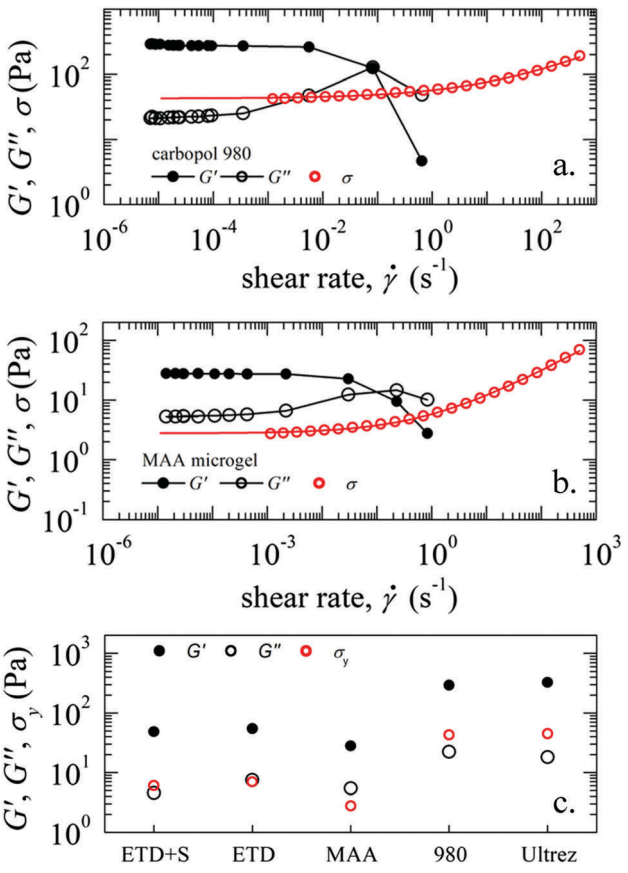

Fig. 12 Superimposed unidirectional/oscillatory shearing. (a and b) Oscillatory rheology at 1 Hz frequency and 1% strain amplitude is performed on packed microgels while simultaneously applying a unidirectional shear. At low shear rates, the elastic moduli remain higher than the viscous moduli. G' and G'' cross in the regime where unidirectional shear stress rises. (c) For all types of microgels used in this study, we find that $G' > G''$ at low shear rates (10^{-5} s^{-1} data shown).

results suggest that the mixing protocol used for samples discussed in the manuscript body are not significantly affecting our rheological measurements through microgel deterioration.

Superimposed unidirectional/oscillatory shearing tests

To test whether packed microgels may be described as solid-like under unidirectional shearing at low shear rates, we perform oscillatory rheology at 1 Hz and 1% applied strain superimposed with unidirectional shear at many shear rates. We find the elastic moduli measured with this test are always higher than the viscous moduli at low shear rates, where our purely unidirectional shear tests exhibit a plateau in shear stress. With increasing shear rate, where the unidirectional shear stress begins to rise, G' and G'' cross, entering a fluid-like regime (Fig. 12).

Author contributions

T. B. and T. E. A. developed the scaling concepts of jammed microgel yielding. T. B. prepared all jammed microgel samples and performed the rheological experiments. C. P. K., C. S. O. and, B. S. S. synthesized the MAA microgels. J. M. U. and W. G. S. measured the friction coefficient between two MAA hydrogel surfaces. T. B. and T. E. A. wrote the manuscript.

Acknowledgements

This material is based upon work supported by the National Science Foundation under Grant No. DMR-1352043'.

References

1 K. Pham, G. Petekidis, D. Vlassopoulos, S. Egelhaaf, W. Poon and P. Pusey, *J. Rheol.*, 2008, **52**, 649–676.
2 A. Fernandez-Nieves, H. Wyss, J. Mattsson and D. A. Weitz, *Microgel suspensions: fundamentals and applications*, John Wiley & Sons, 2011.
3 C. Pellet and M. Cloitre, *Soft Matter*, 2016, **12**, 3710–3720.
4 D. A. Sessoms, I. Bischofberger, L. Cipelletti and V. Trappe, *Philos. Trans. R. Soc. London, Ser. A*, 2009, **367**, 5013–5032.
5 G. Ovarlez, Q. Barral and P. Coussot, *Nat. Mater.*, 2010, **9**, 115–119.
6 I. A. Gutowski, D. Lee, J. R. de Bruyn and B. J. Frisken, *Rheol. Acta*, 2012, **51**, 441–450.
7 P. I. Barker, N. A. Ziskin and M. J. Grossfeld, Multiphase cosmetic composition, *US 4335103 A*, 1982.
8 O. Sonneville-Aubrun, J.-T. Simonnet and F. L'alloret, *Adv. Colloid Interface Sci.*, 2004, **108**, 145–149.
9 K. Timm, C. Myant, H. Spikes and M. Grunze, *Tribol. Int.*, 2011, **44**, 1695–1703.
10 J. B. Thorne, G. J. Vine and M. J. Snowden, *Colloid Polym. Sci.*, 2011, **289**, 625.
11 B. R. Saunders and B. Vincent, *Adv. Colloid Interface Sci.*, 1999, **80**, 1–25.
12 D. Saatweber and B. Vogt-Birnbrich, *Prog. Org. Coat.*, 1996, **28**, 33–41.
13 T. Bhattacharjee, C. J. Gil, S. L. Marshall, J. M. Urueña, C. S. O'Bryan, M. Carstens, B. Keselowsky, G. D. Palmer, S. Ghivizzani and C. P. Gibbs, *ACS Biomater. Sci. Eng.*, 2016, **2**, 1787–1795.
14 T. Bhattacharjee, S. M. Zehnder, K. G. Rowe, S. Jain, R. M. Nixon, W. G. Sawyer and T. E. Angelini, *Sci. Adv.*, 2015, **1**, e1500655.
15 K. J. LeBlanc, S. R. Niemi, A. I. Bennett, K. L. Harris, K. D. Schulze, W. G. Sawyer, C. Taylor and T. E. Angelini, *ACS Biomater. Sci. Eng.*, 2016, **2**, 1796–1799.
16 Y. Jin, A. Compaan, T. Bhattacharjee and Y. Huang, *Biofabrication*, 2016, **8**, 025016.
17 T. J. Hinton, A. Hudson, K. Pusch, A. Lee and A. W. Feinberg, *ACS Biomater. Sci. Eng.*, 2016, **2**, 1781.
18 C. S. O'Bryan, T. Bhattacharjee, S. Hart, C. P. Kabb, K. D. Schulze, I. Chilakala, B. S. Sumerlin, W. G. Sawyer and T. E. Angelini, *Sci. Adv.*, 2017, **3**, e1602800.
19 D. Bonn, J. Paredes, M. M. Denn, L. Berthier, T. Divoux and S. Manneville, arXiv preprint arXiv:1502.05281, 2015.
20 Z. Shao, A. S. Negi and C. O. Osuji, *Soft Matter*, 2013, **9**, 5492–5500.
21 P. Coussot and G. Ovarlez, *Eur. Phys. J. E: Soft Matter Biol. Phys.*, 2010, **33**, 183–188.
22 T. Mason, J. Bibette and D. Weitz, *J. Colloid Interface Sci.*, 1996, **179**, 439–448.
23 L. Mohan, C. Pellet, M. Cloitre and R. Bonnecaze, *J. Rheol.*, 2013, **57**, 1023–1046.
24 J. R. Seth, L. Mohan, C. Locatelli-Champagne, M. Cloitre and R. T. Bonnecaze, *Nat. Mater.*, 2011, **10**, 838–843.
25 G. Romeo and M. P. Ciamarra, *Soft Matter*, 2013, **9**, 5401–5406.
26 P. Menut, S. Seiffert, J. Sprakel and D. A. Weitz, *Soft Matter*, 2012, **8**, 156–164.
27 P. J. Flory, *Principles of polymer chemistry*, Cornell University Press, 1953.
28 P.-G. de Gennes, *Scaling Concepts in Polymer Physics*, Cornell University Press, 1979.
29 R. Colby and M. Rubinstein, *Polymer Physics*, Oxford University, New-York, 2003, pp. 274–281.
30 A. V. Dobrynin, R. H. Colby and M. Rubinstein, *Macromolecules*, 1995, **28**, 1859–1871.
31 M. Rubinstein, R. H. Colby and A. V. Dobrynin, *Phys. Rev. Lett.*, 1994, **73**, 2776.
32 M. Rubinstein, R. H. Colby, A. V. Dobrynin and J.-F. Joanny, *Macromolecules*, 1996, **29**, 398–406.
33 A. Khokhlov and K. Khachaturian, *Polymer*, 1982, **23**, 1742–1750.
34 S. L. Carnie, G. A. Christos and T. P. Creamer, *J. Chem. Phys.*, 1988, **89**, 6484–6496.
35 G. A. Christos, S. L. Carnie and T. P. Creamer, *Macromolecules*, 1992, **25**, 1121–1124.
36 T. Barenbrug, J. Smit and D. Bedeaux, *Macromolecules*, 1993, **26**, 6864–6872.
37 J. Barrat and D. Boyer, *J. Phys. II*, 1993, **3**, 343–356.
38 W. H. Herschel and R. Bulkley, *Colloid Polym. Sci.*, 1926, **39**, 291–300.
39 R. T. Bonnecaze and M. Cloitre, *High Solid Dispersions*, Springer, 2010, pp. 117–161.

40 J. M. Urueña, A. A. Pitenis, R. M. Nixon, K. D. Schulze, T. E. Angelini and W. G. Sawyer, *Biotribology*, 2015, **1**, 24–29.
41 W. G. Sawyer, K. D. Freudenberg, P. Bhimaraj and L. S. Schadler, *Wear*, 2003, **254**, 573–580.
42 A. Fernandez-Barbero, A. Fernandez-Nieves, I. Grillo and E. Lopez-Cabarcos, *Phys. Rev. E: Stat., Nonlinear, Soft Matter Phys.*, 2002, **66**, 051803.
43 F. K. Oppong, L. Rubatat, B. J. Frisken, A. E. Bailey and J. R. de Bruyn, *Phys. Rev. E: Stat., Nonlinear, Soft Matter Phys.*, 2006, **73**, 041405.
44 D. Lee, I. A. Gutowski, A. E. Bailey, L. Rubatat, J. R. de Bruyn and B. J. Frisken, *Phys. Rev. E: Stat., Nonlinear, Soft Matter Phys.*, 2011, **83**, 031401.
45 P.-G. De Gennes, *Simple views on condensed matter*, World Scientific, 2003.
46 F. Brochard and P. De Gennes, *Europhys. Lett.*, 1986, **1**, 221.
47 A. A. Pitenis, J. M. Urueña, A. C. Cooper, T. E. Angelini and W. G. Sawyer, *J. Tribol.*, 2016, **138**, 042103.
48 J. J. Liétor-Santos, B. Sierra-Martín and A. Fernández-Nieves, *Phys. Rev. E: Stat., Nonlinear, Soft Matter Phys.*, 2011, **84**, 060402.
49 I. B. De Aguiar, T. Laar, M. Meireles, A. Bouchoux, J. Sprakel and K. Schroën, *Sci. Rep.*, 2017, **7**, 10223.
50 C. J. Dimitriou, R. H. Ewoldt and G. H. McKinley, *J. Rheol.*, 2013, **57**, 27–70.
51 B. C. Blackwell and R. H. Ewoldt, *J. Non-Newtonian Fluid Mech.*, 2016, **227**, 80–89.
52 N. Denkov, S. Tcholakova, K. Golemanov and A. Lips, *Phys. Rev. Lett.*, 2009, **103**, 118302.
53 M. Pelaez-Fernandez, A. Souslov, L. Lyon, P. M. Goldbart and A. Fernandez-Nieves, *Phys. Rev. Lett.*, 2015, **114**, 098303.
54 A. Scotti, U. Gasser, E. S. Herman, M. Pelaez-Fernandez, J. Han, A. Menzel, L. A. Lyon and A. Fernández-Nieves, *Proc. Natl. Acad. Sci. U. S. A.*, 2016, **113**, 5576–5581.
55 B. Géraud, L. Jørgensen, C. Ybert, H. Delanoë-Ayari and C. Barentin, *Eur. Phys. J. E: Soft Matter Biol. Phys.*, 2017, **40**, 5.
56 J. A. Cobb, A. C. Dunn, J. Kwon, M. Sarntinoranont, W. G. Sawyer and R. Tran-Son-Tay, *Biotechnol. Lett.*, 2008, **30**, 801–806.
57 P. L. Dickrell, S. B. Sinnott, D. W. Hahn, N. R. Raravikar, L. S. Schadler, P. M. Ajayan and W. G. Sawyer, *Tribol. Lett.*, 2005, **18**, 59–62.
58 A. C. Rennie, P. L. Dickrell and W. G. Sawyer, *Tribol. Lett.*, 2005, **18**, 499–504.
59 A. C. Dunn, T. D. Zaveri, B. G. Keselowsky and W. G. Sawyer, *Tribol. Lett.*, 2007, **27**, 233–238.
60 A. C. Dunn, W. G. Sawyer and T. E. Angelini, *Tribol. Lett.*, 2014, **54**, 59–66.
61 A. C. Dunn, J. A. Cobb, A. N. Kantzios, S. J. Lee, M. Sarntinoranont, R. Tran-Son-Tay and W. G. Sawyer, *Tribol. Lett.*, 2008, **30**, 13.
62 B. A. Krick, J. R. Vail, B. N. J. Persson and W. G. Sawyer, *Tribol. Lett.*, 2012, **45**, 185–194.
63 A. Pitenis, J. Uruena, K. Schulze, R. Nixon, A. Dunn, B. Krick, W. Sawyer and T. Angelini, *Soft Matter*, 2014, **10**, 8955–8962.
64 R. Skouri, F. Schosseler, J. Munch and S. Candau, *Macromolecules*, 1995, **28**, 197–210.

